

Polaron dynamics in two-dimensional photon-echo spectroscopy of molecular rings

Thanh Duc Huynh,¹ Ke-Wei Sun,^{1,2} Maxim Gelin,³ and Yang Zhao^{1,a)}

¹*School of Materials Science and Engineering, Nanyang Technological University, Singapore 639798*

²*School of Science, Hangzhou Dianzi University, Hangzhou 310018, China*

³*Department of Chemistry, Technische Universität München, Garching D-85747, Germany*

(Received 12 May 2013; accepted 20 August 2013; published online 10 September 2013)

We have developed a new approach to the computation of third-order spectroscopic signals of molecular rings, by incorporating the Davydov soliton theory into the nonlinear response function formalism. The Davydov D_1 and \tilde{D} Ansatzes have been employed to treat the interactions between the excitons and the primary phonons, allowing for a full description of arbitrary exciton-phonon coupling strengths. As an illustration, we have simulated a series of optical 2D spectra for two models of molecular rings. © 2013 AIP Publishing LLC. [<http://dx.doi.org/10.1063/1.4820135>]

I. INTRODUCTION

Solar to chemical energy conversion in photosynthesis is one of the most important biological processes. Specialized light harvesting complexes in bacteria and green plants are well-known to harvest and transfer solar energy to photochemical reaction centers (RC) with nearly 100% efficiency.^{1–3} Central to the energy transfer process in photosynthetic machinery are aggregates of pigments that serve as antenna as well as a transport network for excitons generated by solar photons. In purple bacteria, for example, they are found in the form of rings comprised of sixteen to thirty four pigments. The B850 ring in purple bacteria, also called the light harvesting complex II (LH2), consists of 16 tightly positioned bacteriochlorophylls-a (BChls-a), with the Mg–Mg distance about 9.36 Å for the $1\alpha - 1\beta$ dimer, and about 8.78 Å for the $2\alpha - 1\beta$ dimer.⁴ Molecules forming such rings generally interact with a bath consisting of nuclear degrees of freedom. The intra-ring dynamics is usually described by the Holstein model,⁵ in which the vibrations of the molecules generate high frequency phonon modes that may undergo coherent oscillatory motion. On the other hand, the surroundings of the ring (such as water and protein matrix) are generally modeled by a continuous distribution of oscillators that yield irreversible relaxation.⁶

Nonlinear femtosecond optical spectroscopy is one of the major sources of information on the functioning of photosynthetic systems.^{7,8} With recent technological advances, the technique of two-dimensional (2D) electronic spectroscopy has emerged as a highly sophisticated tool for studying excitonic relaxation and dephasing in a variety of molecular and biological systems.^{9–24} Coherent and incoherent exciton dynamics in H- or J-type aggregates and in light-harvesting complexes can be probed by various optical measurements such as time-resolved fluorescence,^{12,25,26} pump-probe,^{27–29} photon echoes,^{30–32} 2D electronic spectroscopy,^{9,15,18–22} and 2D infrared spectroscopy.^{13,33–35} The availability of nonlinear

optical responses has also enormously enriched our knowledge on the role of disorder in molecular transitions and the effects caused by multiexciton interactions.^{11,14}

The information delivered by various spectroscopic techniques is encoded into the third-order optically induced polarization $P^{(3)}(t)$. There exist a variety of theoretical methods for the simulation of $P^{(3)}(t)$ (see Refs. 6–9 and 36–40 for recent reviews). They can broadly be subdivided into the perturbative and the nonperturbative approaches. The idea of the nonperturbative approach is to incorporate all relevant laser fields into the system Hamiltonian (which thus becomes time-dependent), and to numerically calculate the dynamics of the driven system.^{39,40} For example, the nonperturbative approach can be combined with multiconfigurational time-dependent Hartree (MCTDH) method,⁴¹ which is one of the most powerful currently available methods for computing many-body quantum dynamics, allowing for the fully quantum mechanical calculation of steady-state⁴² and femtosecond four-wave-mixing^{43,44} optical signals.

The most popular and mature is, however, the perturbative approach, in which the field-matter interactions are treated perturbatively, and $P^{(3)}(t)$ is expressed as a triple time integral involving the third-order response functions.^{6,9,36} The response functions can be evaluated analytically and exactly for the multilevel displaced Brownian oscillator model.⁶ The model comprises several electronic states with the multimode shifted harmonic potential energy surfaces, yielding a “zero order” description for many materials systems. For describing complex systems with interstate (excitonic) couplings, we have to go beyond that description. A common practice is to adopt the system-bath partitioning, and this is where theoretical nonlinear spectroscopy meets theory of open quantum systems and quantum master equations (QMEs).^{45,46} Due to the enormous complexity of photosynthetic systems, the interpretation of the results is however still a huge challenge, and the validity of the exciton approach when subjected to the coupling to different types of baths ranging from water to proteins is contentious. Proper interpretation of measured signals and extraction of useful

^{a)}Electronic mail: YZhao@ntu.edu.sg

information out of them are virtually impossible without adequate theoretical support. If the bath dynamics is faster than that of the system, one can consider the bath as Markovian and neglect the memory effects in the reduced system dynamics. If the system dynamics is faster than (or comparable to) that of the bath, one has to resort to a non-Markovian description. Non-Markovian QMEs provide finer details of the excitonic dynamics.^{10,47–50} It is well known that the Markovian exciton theory leads to the Lorentzian lineshapes, while non-Markovian processes yield more complicated lineshapes.^{6,11,12}

In a functional photosynthetic system, transport properties can be studied via modeling of a quasiparticle called polaron, which comprises an exciton coupled to its surrounding phonon cloud. Since the exciton-phonon coupling in such systems is typically not weak, the applicability of the QME with second-order perturbative truncation such as the Redfield equation may be rendered invalid. The small-polaron transformation⁵¹ extends the domain of validity of the Redfield equation towards stronger system-bath couplings,^{52–55} but does not allow yet for arbitrary coupling strengths. On the other hand, the path integral formalism allows us to handle strong system-bath coupling by introducing the Feynman-Vernon influence functional. This method has earlier been employed to study the nonperturbative equation of motion in various light-harvesting complexes.^{47–50} Existing nonperturbative results are limited to comparatively small systems. Recently, some progress was made in calculating LH2 ring by using a scaled hierarchical equation of motion (HEOM) approach, which can be applied to systems with 18 or fewer pigments.⁵⁶ Furthermore, it is commonly assumed that phonon degrees of freedom are at thermal equilibrium before the optical pulses come. This assumption may not be fulfilled while dealing with fast exciton dynamics (hundreds of fs) and strong exciton-phonon coupling.

In order to circumvent aforementioned difficulties, the Dirac-Frenkel time-dependent variational method has been adopted by a number of authors to investigate the real-time dynamics of the Davydov *Ansätze*.^{57–62} Using the same computationally efficient approach, we have previously calculated with sufficient precision the detailed inter- and intra-ring dynamics of LH2 rings in purple bacteria.^{63,64} In this work, two trial states from the hierarchy of Davydov *Ansätze*, namely, the Davydov D_1 and \bar{D} trial states, are used to simulate the intra-ring dynamics of a single B850 ring. The two *Ansätze* have been shown to yield accurate results when describing the excitonic dynamics over a wide range of the exciton-phonon coupling strength.^{61,62,64,65} The primary phonons in the B850 ring are believed to be in the range of 1500 cm^{-1} ,⁶⁶ which justifies a zero-temperature treatment in studying the exciton dynamics. The secondary continuous phonons can be attributed to the protein matrix and have much lower energies. The secondary phonons can thus be viewed as a channel for relaxation and can be treated by the lineshape method.

In the present paper, we incorporate the description of the system dynamics in terms of the Davydov *Ansätze* into the framework of nonlinear response functions. The rest of the paper is organized as follows: Section II comprises the model and the methodology employed in this work. As an

illustration, Sec. III displays and discusses simulation results of optical 2D spectra for two model J-aggregates, in which the transition dipoles are tangentially oriented. Our main results are briefly summarized in Sec. IV.

II. METHODOLOGY

A. Model system

We consider a one-dimensional molecular ring constructed by N interacting molecules (such as BChls-a) embedded in a protein environment. The total Hamiltonian for this model can be written as

$$H = H_S + H_B + H_{SB}. \quad (1)$$

There exist two major approaches to the system-bath partitioning in excitonic systems (see Refs. 8, 36, and 67–71 for a comprehensive discussion). In the first approach, a few high-frequency vibrational modes with strong exciton-phonon coupling are incorporated into the system Hamiltonian and treated explicitly. The rest of the vibrational modes are assumed to form a heat bath. The bath is normally treated as harmonic, with bilinear system-bath coupling. In the second approach, all vibrational modes are incorporated into the bath. The two models of the exciton transport are, in principle, equivalent. Via a canonical transformation, on the one hand, we can switch from one description to the other by incorporating the system modes into the bath or by singling-out several (high-frequency) modes from the bath and treating them explicitly. On the other hand, the more vibrational modes with strong exciton-phonon coupling are incorporated into the system Hamiltonian, the simpler is the bath spectral density, and the weaker (in general) is the system-bath coupling.

In the present paper, we follow the first approach. The first term in Eq. (1) is a Holstein Hamiltonian describing excitations in the molecular ring:⁷²

$$H_S = H_{\text{ex}} + H_{\text{ph}} + H_{\text{ex-ph}}. \quad (2)$$

Here, H_{ex} is the Frenkel-exciton Hamiltonian,

$$H_{\text{ex}} = \varepsilon_g |g\rangle\langle g| + \sum_{m=1}^N \varepsilon_m |m\rangle\langle m| + \sum_{m=1}^N \sum_{n \neq m}^N J_{nm} |n\rangle\langle m|, \quad (3)$$

$\varepsilon_g \equiv 0$ is the energy in the ground excitonic state, ε_m is the excitation energy of the molecule m , $|m\rangle$ is the state in which only the molecule m is excited, and J_{nm} is the coupling between the molecules n and m . H_{ph} is the phonon Hamiltonian which describes the primary vibrations of the molecular ring

$$H_{\text{ph}} = \sum_q \hbar \omega_q b_q^\dagger b_q, \quad (4)$$

and $H_{\text{ex-ph}}$ is responsible for the exciton-phonon coupling which is assumed to be site-diagonal:

$$H_{\text{ex-ph}} = \sum_q \sum_{m=1}^N g_q \hbar \omega_q (b_q e^{-iqm} + b_q^\dagger e^{iqm}) |m\rangle\langle m|. \quad (5)$$

b_q (b_q^\dagger) denotes the annihilation (creation) operator of the primary phonon with frequency ω_q , g_q is the exciton-phonon coupling strength, and dimensionless momentum is denoted

by $q = 2\pi n_q/N$ ($n_q = -7, -6, \dots, 8$), where $N = 16$. We assume a linear dispersion for the primary phonon,

$$\omega_q = \omega_0 + 2W(|q|/\pi - 1/2), \quad (6)$$

and consider the elliptic form of the phonon bath correlation function,

$$\begin{aligned} C_{00}(\omega) &= \frac{1}{N} \sum_q g_q^2 \omega_q^2 \delta(\omega - \omega_q) \\ &= \frac{2S\omega^2}{N\pi W^2} \sqrt{W^2 - (\omega - \omega_0)^2}. \end{aligned} \quad (7)$$

Here, ω_0 is the central phonon frequency and W is the frequency bandwidth. The exciton-phonon coupling can conveniently be characterized via the Huang-Rhys factor S defined by the relation

$$\frac{1}{N} \sum_q g_q^2 \omega_q = S\omega_0. \quad (8)$$

Here, g_q can be obtained from Eqs. (6)–(8) for a given Huang-Rhys factor S and a phonon bandwidth W .⁶¹

The second and the third terms in Eq. (1) describe interaction of H_S with “the rest of the world,” viz., with the low-frequency intramolecular vibrations of BChls-a and with nuclear degrees of freedom of the environment. Having incorporated the vibrational modes with strong exciton-phonon coupling into H_S , we may utilize a rather simplified description of H_B and H_{SB} , since they are responsible for (relatively long time) population decays and dephasings. Motivated by the symmetry of the molecular ring, we assume a harmonic bath with site-independent system-bath couplings,

$$H_B = \sum_j \hbar \Omega_j a_j^\dagger a_j, \quad (9)$$

$$H_{SB} = \sum_j \sum_{m=1}^N \kappa_j \hbar \Omega_j (a_j + a_j^\dagger) |m\rangle \langle m|. \quad (10)$$

Here, a_j (a_j^\dagger) is the annihilation (creation) operator of a phonon of the bath with frequency Ω_j , and κ_j is the exciton-bath coupling strength of the j th bath mode. The bath spectral density is determined by

$$D(\omega) = \sum_j \kappa_j^2 \Omega_j^2 \delta(\omega - \Omega_j). \quad (11)$$

B. Response functions and 2D spectroscopy

To simulate optical 2D spectra, we employ the nonlinear response function approach as reviewed in Refs. 9 and 36. We define the field-matter interaction Hamiltonian in the dipole approximation and in the rotating wave approximation as follows:

$$\begin{aligned} H_F(t) &= - \sum_{a=1}^3 \sum_{m=1}^N E_a(t - \tau_a) e^{i\mathbf{k}_a \mathbf{r} - \omega_a(t - \tau_a)} \mathbf{e}_a \boldsymbol{\mu}_m |m\rangle \langle g| \\ &+ H.c., \end{aligned} \quad (12)$$

Here \mathbf{e}_a , \mathbf{k}_a , ω_a , $E_a(t)$, and τ_a denote the polarization, wave vector, carrier frequency, dimensionless envelope, and the central time of the pulses. $\boldsymbol{\mu}_m$ is the matrix element of the transition dipole moment between the excitonic ground state $|g\rangle$ and an excitonic excited state $|m\rangle$ (for simplicity, we assume $|\boldsymbol{\mu}_m| = \mu$).

It is common to define the pulse arrival times in the system-field Hamiltonian (12) as follows:

$$\tau_1 = -T - \tau, \quad \tau_2 = -T, \quad \tau_3 = 0, \quad (13)$$

where τ (the so-called coherence time) is the delay time between the second and the first pulse, and T (the so-called population time) is the delay time between the third and the second pulse. Before the optical excitation ($t \ll -T - \tau$), the system is assumed to be in its global ground state $|g\rangle|0\rangle_{\text{ph}}$ ($|0\rangle_{\text{ph}}$ is the vacuum state of the primary phonons), while the heat bath is in thermal equilibrium at temperature T_{eq} . Adopting this factorized initial condition, we neglect correlations between the primary system and the “rest of the world.” This is not a severe assumption, since all strong interactions and correlations are incorporated into the primary system described by Hamiltonian (2).

After the Hamiltonians (1) and (12) have been defined, the third-order optically induced polarization $P^{(3)}(t)$ can be (formally) expressed in terms of the nonlinear response functions R_i , $i = 1-4$.^{6,9,36} To evaluate the photon echo signal, we need the component of $P^{(3)}(t)$ in the direction $-\mathbf{k}_1 + \mathbf{k}_2 + \mathbf{k}_3$, which yields the so-called rephasing (subscript R) contribution $P_R^{(3)}(t)$, as well as the component of $P^{(3)}(t)$ in the direction $\mathbf{k}_1 - \mathbf{k}_2 + \mathbf{k}_3$, which yields the so-called non-rephasing (subscript NR) contribution $P_{NR}^{(3)}(t)$. Assuming that the pulse durations are much shorter than all relevant system and bath times, we can substitute the pulse envelopes $E_a(t - \tau_a)$ by delta-functions (the so-called impulsive limit). We can then write,

$$P_R^{(3)}(\tau, T, t) \sim -i [R_2(\tau, T, t) + R_3(\tau, T, t)] \quad (14)$$

and

$$P_{NR}^{(3)}(\tau, T, t) \sim -i [R_1(\tau, T, t) + R_4(\tau, T, t)]. \quad (15)$$

Once the polarizations (14) and (15) are known, the rephasing and non-rephasing 2D photon echo spectra are evaluated by two-dimensional Fourier-Laplace transforms as follows:

$$\begin{aligned} S_R(\omega_\tau, T, \omega_t) &= \text{Re} \int_0^\infty \int_0^\infty dt d\tau i P_R^{(3)}(\tau, T, t) e^{-i\omega_\tau \tau + i\omega_t t}, \end{aligned} \quad (16)$$

$$\begin{aligned} S_{NR}(\omega_\tau, T, \omega_t) &= \text{Re} \int_0^\infty \int_0^\infty dt d\tau i P_{NR}^{(3)}(\tau, T, t) e^{i\omega_\tau \tau + i\omega_t t}. \end{aligned} \quad (17)$$

The total 2D signal is defined by the sum of the two,

$$S(\omega_\tau, T, \omega_t) = S_R(\omega_\tau, T, \omega_t) + S_{NR}(\omega_\tau, T, \omega_t). \quad (18)$$

The response functions R_i are defined in the standard way (see Refs. 9 and 36) in terms of the projections of the total Hamiltonian (1) onto the excitonic ground state $|g\rangle$, and onto the

manifold of the singly excited electronic states $\{|m\rangle\}$. To evaluate these response functions, we start from considering the impact of the external vibrational bath (9). It is important to realize that the system-bath Hamiltonian (Eq. (10)) commutes with the system Hamiltonian (Eq. (2)). In such a case, the bath degrees of freedom can be traced out analytically, yielding an exact master equation for the reduced (system) density matrix.^{74,75} As for the response functions, we can additionally make use of the fact that the system-bath coupling is the same for all excitons. Thus, the bath-induced relaxation and dephasing are accounted for exactly through the lineshape factors F_i within the second-order cummulant expansion. We therefore obtain

$$R_1(\tau, T, t) = F_1(\tau, T, t) \sum_{n, n', n'', n'''} C_{n, n', n'', n'''} \text{ph}\langle 0 | \langle n | e^{\frac{i}{\hbar} H_S T} | n' \rangle \langle n'' | e^{-\frac{i}{\hbar} H_S (\tau + T + t)} | n''' \rangle | 0 \rangle_{\text{ph}},$$

$$R_2(\tau, T, t) = F_2(\tau, T, t) \sum_{n, n', n'', n'''} C_{n, n', n'', n'''} \text{ph}\langle 0 | \langle n | e^{\frac{i}{\hbar} H_S (\tau + T)} | n' \rangle \langle n'' | e^{-\frac{i}{\hbar} H_S (\tau + T)} | n''' \rangle | 0 \rangle_{\text{ph}},$$
(19)

$$R_3(\tau, T, t) = F_3(\tau, T, t) \sum_{n, n', n'', n'''} C_{n, n', n'', n'''} \text{ph}\langle 0 | \langle n | e^{\frac{i}{\hbar} H_S \tau} | n' \rangle \langle n'' | e^{-\frac{i}{\hbar} H_S t} | n''' \rangle | 0 \rangle_{\text{ph}},$$

$$R_4(\tau, T, t) = F_4(\tau, T, t) \sum_{n, n', n'', n'''} C_{n, n', n'', n'''} \text{ph}\langle 0 | \langle n | e^{-\frac{i}{\hbar} H_S t} | n' \rangle \langle n'' | e^{-\frac{i}{\hbar} H_S \tau} | n''' \rangle | 0 \rangle_{\text{ph}}.$$

Here,

$$C_{n, n', n'', n'''} = (\mathbf{e}_1 \boldsymbol{\mu}_n)(\mathbf{e}_2 \boldsymbol{\mu}_{n'}) (\mathbf{e}_3 \boldsymbol{\mu}_{n''}) (\mathbf{e}_4 \boldsymbol{\mu}_{n'''}) \quad (20)$$

are the geometrical factors which must be averaged over the orientations of the transition dipole moments $\boldsymbol{\mu}_n$. If reorientation of $\boldsymbol{\mu}_n$ can be neglected on the timescale of the experiment, the (static) orientational averaging can be done analytically (see, e.g., Refs. 76 and 77). Denoting the averaging by overbar and assuming, for simplicity, that all laser beams possess the same polarization, we obtain

$$\bar{C}_{n, n', n'', n'''} = \frac{1}{15} ((\boldsymbol{\mu}_n \boldsymbol{\mu}_{n'}) (\boldsymbol{\mu}_{n''} \boldsymbol{\mu}_{n'''})) + (\boldsymbol{\mu}_n \boldsymbol{\mu}_{n''}) (\boldsymbol{\mu}_{n'} \boldsymbol{\mu}_{n'''}) + (\boldsymbol{\mu}_n \boldsymbol{\mu}_{n'''}) (\boldsymbol{\mu}_{n'} \boldsymbol{\mu}_{n''}).$$
(21)

While evaluating the response functions, the coefficients \bar{C} [Eq. (21)] should be inserted instead of C [Eq. (20)].

The system propagators $e^{\frac{i}{\hbar} H_S T}$ in Eqs. (19) describe coherent dynamics of the molecular ring, while the lineshape

factors F_i are explicitly defined as follows:^{6,9,36}

$$F_1(\tau, T, t) = e^{-g^*(t) - g(\tau) - g^*(T) + g^*(T+t) + g(\tau+T) - g(\tau+T+t)},$$

$$F_2(\tau, T, t) = e^{-g^*(t) - g^*(\tau) + g(T) - g(T+t) - g^*(\tau+T) + g^*(\tau+T+t)},$$
(22)

$$F_3(\tau, T, t) = e^{-g(t) - g^*(\tau) + g^*(T) - g^*(T+t) - g^*(\tau+T) + g^*(\tau+T+t)},$$

$$F_4(\tau, T, t) = e^{-g(t) - g(\tau) - g(T) + g(T+t) + g(\tau+T) - g(\tau+T+t)},$$

where $g(t)$ is the lineshape function,

$$g(t) = \int_0^\infty d\omega \frac{D(\omega)}{\omega^2} \times \left[\coth \frac{\hbar\omega}{2k_B T_{eq}} (1 - \cos \omega t) + i (\sin \omega t - \omega t) \right].$$
(23)

A common procedure for the construction of the response functions R_i is as follows.^{9,36} To account for bath-induced relaxation and dephasing, one diagonalizes the system Hamiltonian, evaluates diagonal fluctuations exactly, and treats off-diagonal fluctuations at different levels of approximation. In the present case, due to the symmetry of H_S and H_{SB} , we do not need to diagonalize H_S and resort to additional approximations. This is the first reason for choosing the bath and system-bath coupling Hamiltonians as specified by Eqs. (9) and (10). The second reason rests on physical grounds. The fast vibrational modes with strong exciton-phonon couplings are incorporated into the system Hamiltonian (2) and are accounted for explicitly via the Davydov *Ansätze* (25) and (26). The remaining vibrational modes constituting the bath have relatively low frequencies. It is thus not unreasonable to assume that the BCHs comprising the molecular ring experience concerted fluctuations. Indeed, the bath described by Eqs. (9) and (10) is equivalent to the fully correlated bath (see, e.g., Ref. 71 and references therein), and the bath correlations affect the peak shapes in 2D spectra. In this work, we focus on the application of Davydov *Ansätze* to nonlinear optical spectroscopy rather than on the discrimination between different bath models. The bath of Eqs. (9) and (10) is useful for our purpose, since it yields, without additional approximations, the simple lineshape functions (23) describing the population relaxations and dephasings.

C. The Davydov *Ansätze*

After the bath-induced relaxations have been accounted for, we concentrate on the evaluation of the system propagators in Eqs. (19). Here we come up at the second crucial point in our derivations and substitute the propagators by the corresponding Davydov *Ansätze*,

$$e^{-\frac{i}{\hbar} H_S t} |n\rangle |0\rangle_{\text{ph}} = |\Psi_\sigma(t)\rangle, \quad (24)$$

namely, the Davydov D_1 Ansatz ($\sigma = D_1$) and its simplified version, the \tilde{D} Ansatz ($\sigma = \tilde{D}$).^{61,62} The corresponding trial wave functions take the following forms:

$$|\Psi_{D_1}(t)\rangle = \sum_m \alpha_m(t) |m\rangle \exp \left\{ \sum_q [\lambda_{m,q}(t) \hat{b}_q^\dagger - \text{H.c.}] \right\} |0\rangle_{\text{ph}}, \quad (25)$$

$$|\Psi_{\tilde{D}}(t)\rangle = \sum_{n=1}^N \alpha_n |n\rangle e^{\sum_q (\beta_q e^{-iqn} - \lambda_q) b_q^\dagger - (\beta_q^* e^{iqn} - \lambda_q^*) b_q} |0\rangle_{\text{ph}}. \quad (26)$$

Time-dependent variational parameters α , β , and λ are obtained from solving a set of differential equations generated by the Lagrangian formalism of the Dirac-Frenkel variational method.⁷³ The initial condition we set up for the D_1 Ansatz is that the exciton is located on site $m = 0$ in the molecular ring at $t = 0$, i.e., $\alpha_m(0) = \delta_{m0}$, and there is initially zero phonon displacement over the entire ring, i.e., $\lambda_{mq}(0) = 0$, while for the \tilde{D} Ansatz, we have $\alpha_n(0) = \delta_{n0}$, $\lambda_q(0) = 0$, and $\beta_q(0) = 0$. The reader is referred to the Appendix for more details on the time-dependent variational procedure and on the applications of the Davydov Ansätze to molecular rings.

Before we proceed to the calculation of 2D spectra, it is appropriate to discuss the following two issues:

(i) We have chosen the D_1 and \tilde{D} Ansätze because they account for exciton-phonon correlations, and are thus more suitable for describing the system responses on short laser fields, which can result in optical excitations localized on specific exciton and phonon modes. As has been demonstrated in Refs. 61 and 62, the Ansätze allow us to faithfully reproduce polaron dynamics and linear absorption spectra of cyclic 1D J-aggregates in the broad range of the exciton-phonon and exciton-exciton coupling parameters. As for the application of the Ansätze to the calculation of third-order optical signals, it is crucial to note that the nonlinear response functions (19) are uniquely determined by the propagator (24), which, in turn, is approximated by the Davydov Ansätze (25) and (26). The validity of the Davydov Ansätze (25) and (26) in reproducing the propagator (24) is proven in Refs. 61, 62. This also guarantees their validity in reproducing the response functions (19).

(ii) The Davydov Ansätze D_1 and \tilde{D} describe single-exciton excitations. As a result, we have restricted our analysis to the consideration of the system Hamiltonian (Eq. (2)) in the ground excitonic state $|g\rangle$ and the manifold of the singly excited excitonic states $\{|m\rangle\}$. This level of description is sufficient to treat time- and frequency-resolved spontaneous emission (cf. Ref. 5). Any other four-wave-mixing signal has excited state absorption (ESA) contributions involving higher excited electronic states (for polyatomic molecules) or doubly excited excitonic states (for molecular aggregates). There exist several arguments in favor of neglecting ESA for the molecular rings considered in the present paper. As is well known^{4,66} and explained in Sec. II D, the B850 ring can be regarded with a good accuracy as a two-level excitonic system. Hence, the contribution of the ESA to optical responses of such a system should not be significant. Furthermore, the ESA contributions to 2D signals are sometimes negligible due

to the other reasons (see, e.g., Refs. 78 and 79 on optical 2D spectra of Fenna-Matthews-Olson photosynthetic complex). In addition, as we argue in Sec. III, the calculated 2D responses exhibit many features which are not affected by the ESA. Nevertheless, the 2D signals considered below should be regarded, rigorously speaking, as model signals. *Inter alia*, we have found it elucidating to represent our results as 2D spectra, which reveal Franck-Condon active vibrations through the peaks in the ω_τ , ω_t plane. On the other hand, there are approaches allowing one to construct the Davydov Ansätze for doubly excited excitonic states (see Refs. 80–82 and references therein). Work is in progress to incorporate these approaches into the description of third-order optical signals.

D. Control parameters

Having outlined the general theory, we specify the Hamiltonians which are used in the present work for the calculation of 2D spectra. For the molecular ring, we consider tangentially oriented configuration of the transition dipoles μ_n (head-to-tail). The site energies ε_m in the Hamiltonian (3) are assumed to be identical, i.e., $\varepsilon_m = \varepsilon$. We set $\varepsilon = 0$, meaning that the frequencies ω_t and ω_τ of 2D optical spectra are given relative to the vertical excitation energy ε .

The exciton-exciton coupling is of the form

$$J_{nm} = \begin{pmatrix} 0 & J_1 & W_{1,3} & \cdot & \cdot & \cdot & J_2 \\ J_1 & 0 & J_2 & \cdot & \cdot & \cdot & W_{2,N} \\ W_{3,1} & J_2 & 0 & \cdot & \cdot & \cdot & \cdot \\ \cdot & \cdot & \cdot & \cdot & \cdot & \cdot & \cdot \\ \cdot & \cdot & \cdot & \cdot & 0 & J_2 & W_{N-2,N} \\ \cdot & \cdot & \cdot & \cdot & J_2 & 0 & J_1 \\ J_2 & \cdot & \cdot & \cdot & W_{N,N-2} & J_1 & 0 \end{pmatrix}. \quad (27)$$

Specifically, we consider two models. The toy model (Fig. 1(a)) assumes identical nearest-neighbor couplings $J_1 = J_2 = J$. The realistic model (Fig. 1(b)) describes structural dimerization, implying $J_1 \neq J_2$. Additionally, it includes the dipole-dipole couplings W_{nm} between the n th and m th BChl-a,⁴

$$W_{n,m} = C \left[\frac{\mathbf{d}_n \cdot \mathbf{d}_m}{|\mathbf{r}_{nm}|^3} - \frac{3(\mathbf{d}_n \cdot \mathbf{r}_{nm})(\mathbf{d}_m \cdot \mathbf{r}_{nm})}{|\mathbf{r}_{nm}|^5} \right]. \quad (28)$$

Here C is the proportionality constant, \mathbf{r}_{ij} is the vector connecting the i th and j th monomers, and \mathbf{d}_i are the unit vectors of the transition dipole in the i th BChl-a. In the present work, the following parameters⁴ are adopted: $J_1 = 0.074$ eV, $J_2 = 0.061$ eV, and $C = 79.44$ Å³ eV.

The toy model has a doubly degenerate optically allowed energy state in the lower band with the energy at $-2J \cos(\pm \frac{\pi}{8}) = -0.5543 \hbar \omega_0$. The redshift of spectra is a characteristic feature of J aggregates. The realistic model has two doubly degenerate optically allowed states with the energies $-0.7878 \hbar \omega_0$ and $0.4432 \hbar \omega_0$. The transition dipole moments for the lower degenerate levels are $\mu_l = 1.9320(-2.0648)\mathbf{e}_x + i2.0648(1.9320)\mathbf{e}_y$, while

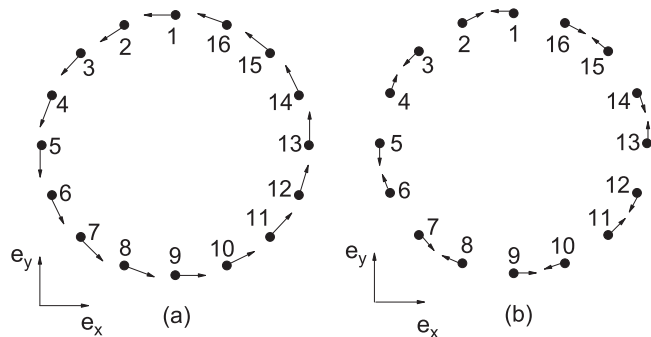


FIG. 1. (a) The toy model of a molecular ring mimicking LH2. Only the nearest-neighbor intermolecular coupling $J_1 = J_2$ is assumed. (b) A realistic model in which structural dimerization is introduced, implying $J_1 \neq J_2$.

those for the upper levels are $\mu_u = 0.0057(-0.0622)\mathbf{e}_x - i0.0622(0.0057)\mathbf{e}_y$, where \mathbf{e}_x and \mathbf{e}_y (unit vectors) label two orthogonal directions in the plane of the B850 ring as shown in Fig. 1. The transition dipole moments for the upper levels are clearly much smaller than those for the lower levels. Therefore, the B850 ring can be approximately regarded as a two-level system. This lends strong support to neglecting the doubly excited excitonic states in the system Hamiltonian (2).

Our choice of two different models of molecular rings is motivated by the following arguments. Recently, effects related to vibrational coherent dynamics have unambiguously been detected in optical 2D spectra of various molecular species.^{83–85} The question of how to distinguish between electronic and vibrational oscillations in peak intensities in 2D spectra is under active debate.^{86–91} In order to check if the Davydov *Ansätze* grasp vibrational features in 2D spectra of molecular rings, the averaged primary phonon energy $\hbar\omega_0$ in Eq. (6) in the toy model is fixed to a low value of 0.05 eV: BChls *a* possess a number of Franck-Condon active vibrations in the spectral range of ~ 0.01 – 0.1 eV.^{92–94} In addition, the analysis of whole body of available spectroscopic data on the B850 band of LH2 yields the bath spectra densities (involving all internal and environmental nuclear degrees of freedom) peaked at several hundreds of wave numbers.^{95,96} As for the realistic model, we set a realistic higher-energy $\hbar\omega_0 = 0.207$ eV.^{66,97} The values of the bandwidth W and the Huang-Rhys factor S are varied.

Two different models of molecular rings stipulate the consideration of two different models of baths of secondary phonons. The toy model emphasizes vibrationally coherent responses and requires more careful description of the phonon bath. Its spectral density (Eq. (11)) is taken in the Drude form

$$D(\omega) = 2\eta \frac{\gamma\omega}{\omega^2 + \gamma^2}, \quad (29)$$

where $\hbar\eta = 0.005$ eV and $\hbar\gamma = 0.003$ eV. The ensuing lineshape functions are evaluated according to Eq. (23) with the inclusion of low-temperature Matsubara terms (see, e.g., Ref. 6). The realistic model treats the B850 band of LH2 in a “realistic” environment with strong electronic dephasing, leading to our choice of simple exponential or Kubo-like lineshape functions.

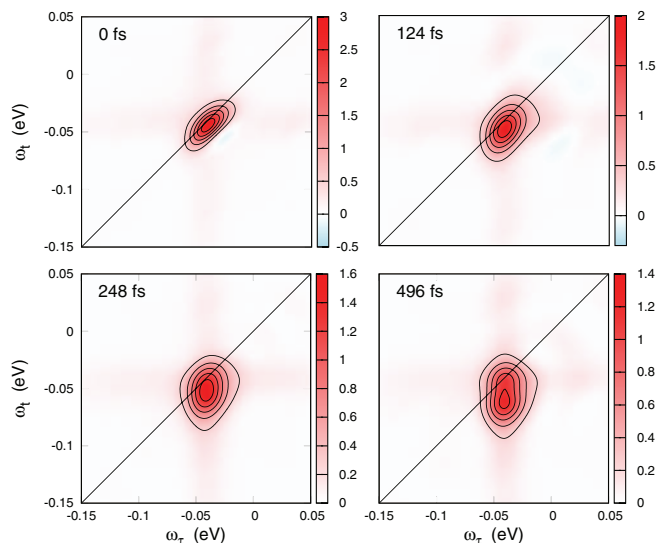


FIG. 2. Time evolution of the 2D spectrum for $S = 0.5$, $W = 0.8\hbar\omega_0$, $J = 0.3\hbar\omega_0$, and $T_{eq} = 50$ K.

2D spectra (16)–(18) were calculated as prescribed by Eqs. (14), (15), and (19). $S(\omega_\tau, T, \omega_t)$ discussed in Sec. III A are evaluated under the assumption that the geometrical factor $\bar{C}_{n,n',n'',n''''}$ (Eq. (21)) can be substituted by an effective constant \bar{C} (several representative calculations with n -dependent $\bar{C}_{n,n',n'',n''''}$ yielded virtually indistinguishable results). $S(\omega_\tau, T, \omega_t)$ discussed in Sec. III B are computed without resorting to the above approximation.

III. RESULTS AND DISCUSSION

A. The Davydov \bar{D} Ansatz

In this section, we present 2D photon-echo spectra $S(\omega_\tau, T, \omega_t)$ computed for a molecular ring with $N = 16$ using the Davydov \bar{D} Ansatz (26). We first consider intermediate exciton-phonon coupling with the Huang-Rhys factor $S = 0.5$, the bandwidth $W = 0.8\hbar\omega_0$, and the transfer integral $J = 0.3\hbar\omega_0$. 2D spectra are shown in Fig. 2 for several population times $T = 0, 3\pi\omega_0^{-1}, 6\pi\omega_0^{-1},$ and $12\pi\omega_0^{-1}$ (0, 124 fs, 248 fs, and 496 fs).

At $T = 0$, the spectrum exhibits a single peak at $\omega_\tau = \omega_t \approx -0.04$ eV. Since the exciton-phonon coupling is rather weak, the spectrum is similar to that of the two-level system. Initially, the peak shape is elliptical and is elongated along the diagonal. As T increases, the peak symmetry axis rotates clockwise, tending to be parallel to the ω_t axis. Besides this dynamic inhomogeneous broadening, the splitting between the absorption peak and the stimulated emission peak due to the population relaxation is also visible. At sufficiently long population time, the spectrum becomes stationary and exhibits the Stokes shift of $2\lambda \approx 0.03$ eV down from the diagonal (λ being the solvent reorganization energy).

Now we consider strong exciton-phonon coupling ($S = 2$) and the associated band narrowing ($W = 0.1\hbar\omega_0$). The corresponding 2D spectra for $J = 0.1\hbar\omega_0$ and $T_{eq} = 50$ K are shown in Fig. 3(a) for several values of the population

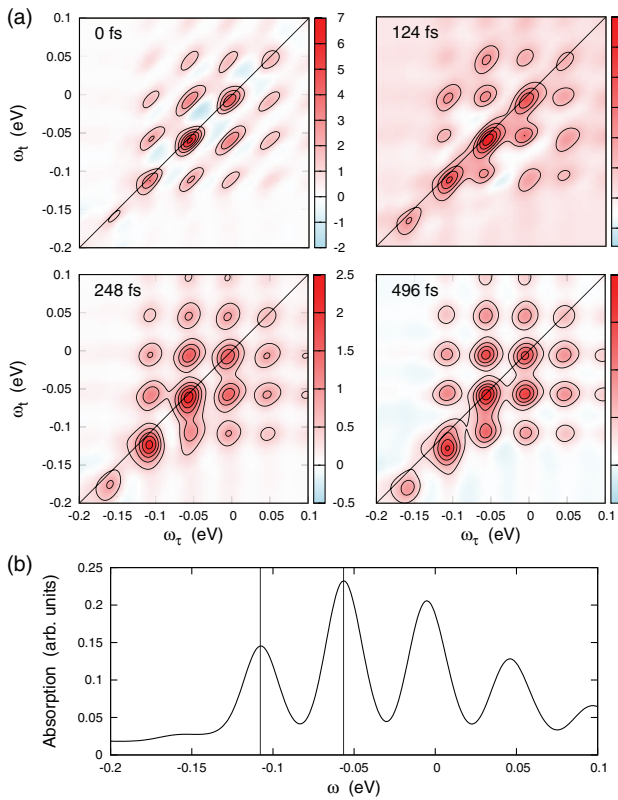


FIG. 3. (a) Time evolution of the 2D spectrum in the case of strong exciton-phonon coupling ($S = 2$) and narrow phonon band ($W = 0.1\hbar\omega_0$) for $J = 0.1\hbar\omega_0$ and $T_{eq} = 50$ K. (b) Linear absorption spectrum.

time T . A multi-peak spectral structure caused by the strong exciton-phonon coupling is clearly observed. Similar vibronic multi-peak patterns show up in 2D signals of many systems: e.g., displaced harmonic oscillators,^{98–101} anharmonic oscillators,¹⁰² systems with avoided crossings,^{103–105} vibronic dimers,¹⁰⁶ and “torsional” dimers.¹⁰⁷

The linear absorption spectrum shown in Fig. 3(b) can be “read out” of the diagonal ($\omega_\tau = \omega_t$) part of the 2D spectrum at $T = 0$. The leftmost peak and the highest intensity peak in Fig. 3(b) correspond to the zero-phonon and the one-phonon sublevels. They are located at $\hbar\omega \approx -0.108$ eV and -0.057 eV, respectively (highlighted by vertical lines). A slight red shift of these peaks from $-S\hbar\omega_0 = -0.1$ eV and $-(S - 1)\hbar\omega_0 = -0.05$ eV is due to the finite J and the presence of the heat bath.

As is seen from Fig. 3(a), the diagonal and off-diagonal peaks may move, as well as change their shape and amplitude with the population time. The time evolution of the peak shapes is similar to that in Fig. 2. The Stokes shifts due to the energy reorganization are also seen. At $T = 0$, the strongest absorption and emission peaks coincide and are located at $\hbar\omega_\tau = \hbar\omega_t = -0.057$ eV. At longer T , the population relaxation moves the highest intensity emission peak down to $(\hbar\omega_\tau, \hbar\omega_t) \approx (-0.108$ eV, -0.138 eV).

To extract further details about the polaron dynamics from the 2D spectra, we analyze the population-time evolution of the peak intensities. The peak intensity evolutions are almost insensitive to the presence of ESA, since they pre-

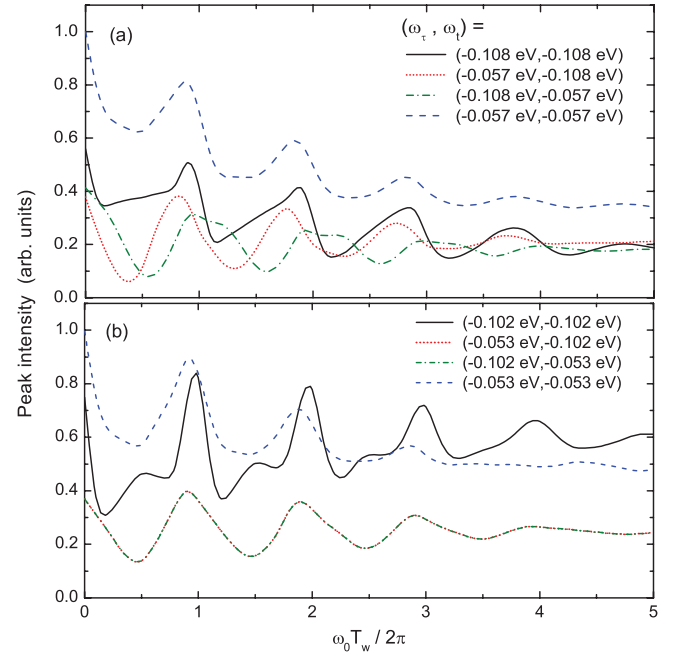


FIG. 4. Time evolutions of diagonal and off-diagonal peaks of the 2D spectrum. Panel (a) is for the Drude bath, while panel (b) is for the corresponding Markovian bath.

dominantly reflect the system dynamics in the singly excited excitonic state. Figure 4 shows T -evolutions of two leftmost diagonal peaks (solid and dashed blue lines) and the corresponding two cross peaks (dotted red and dashed-dotted green lines). The peak intensities are seen to oscillate with the characteristic phonon frequency $\sim\omega_0$. Related vibrational beatings in the population-time dynamics of peaks in 2D optical spectra have been measured.^{83–85}

The peak dynamics are also sensitive to specific mechanisms of bath-induced relaxations. This is clearly demonstrated by the comparison of panels (a) and (b) of Fig. 4. Panel (a) corresponds to the heat bath with the Drude spectral density (11), while panel (b) corresponds to the respective Markovian bath, for which the lineshape factors F_i in Eq. (22) are replaced with $\exp[-\Gamma(\tau + t)]$, where $\Gamma = 0.1\omega_0$ is a phenomenological dephasing constant. Consider T -evolutions of the off-diagonal peaks. In panel (a) the cross peak lying below the diagonal (dotted-red line) gains its amplitude as compared to the other cross peak (dashed-dotted green line). This is a direct consequence of the bath-induced relaxation. In panel (b), the intensities of the two cross peaks are nearly the same. The pure dephasing Markovian bath does not account for excitonic population relaxation, rendering 2D signals symmetrical with respect to the diagonal $\omega_\tau = \omega_t$.

Figure 5 displays the 2D spectra for the population time $T = 12\pi\omega_0^{-1} = 496$ fs at elevating temperatures $T_{eq} = 0, 50, 100,$ and 150 K. As expected, temperature broadens the peak shapes and blurs the multi-peak structure out.

B. The Davydov D_1 Ansatz

We also simulate 2D spectra within a more general D_1 Ansatz. We employ the Markovian bath model which is

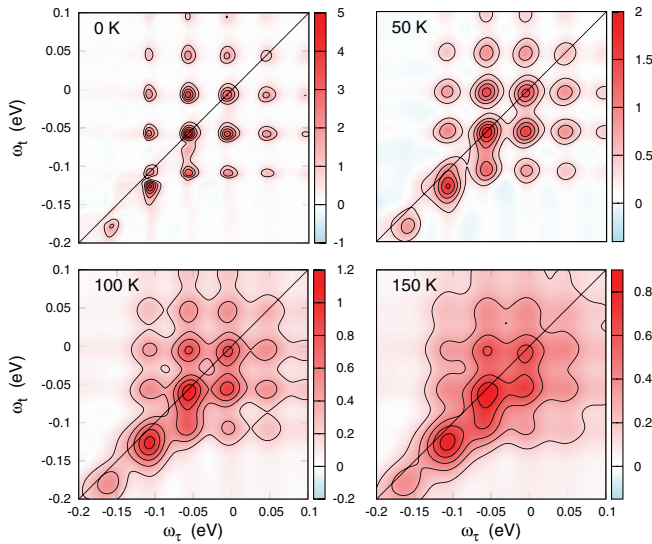


FIG. 5. 2D spectra at the population time $T = 496$ fs for several bath temperatures. Other parameters are the same as in Fig. 3.

similar to the one we used to calculate the peak dynamics in Fig. 4(b), but accounts for a finite lifetime of the singly excited excitonic states. Specifically, we consider the lineshape factors (22) in the form

$$F_i(\tau, T, t) = \exp[-\Gamma(\tau + t) - \Gamma'T], \quad (30)$$

assuming the dephasing rate $\Gamma = 0.1\omega_0$ and the population rate $\Gamma' = 0.06\omega_0$ ($1/\Gamma' = 332$ fs). The spectra at $T = 0$ are plotted in Fig. 6. The left column corresponds to the toy model, while the right column is for the realistic model. The upper, middle, and lower panels correspond to the rephasing, non-rephasing, and total 2D spectra, respectively. Due to rather strong dephasing, the spectra resemble those of a two-level system and reveal only a single peak (cf. Fig. 2). Accordingly, the rephasing (upper panels) and non-rephasing (middle panels) spectra are, approximately, the mirror images of each other. The comparison of spectra in panels (a) and (c) with those in panels (b) and (d) can hardly reveal any difference between the toy and realistic models. On the other hand, the total signals in the lower panels do exhibit certain differences. For example, the star-like shape of the spectrum in Fig. 6(f) is slightly destroyed owing to the contributions of weak transitions to the upper levels with the energy $0.4432\hbar\omega_0$. Therefore, the heat bath does not entirely wash out fine details of the system dynamics. These details may manifest themselves through certain features in 2D signals of molecular rings even under “realistic” conditions.

We have also employed the Davydov D_1 Ansatz for examining the influence of static disorder on 2D signals. The disorder was accounted for by a Gaussian distribution of the (reduced) site energies ε_m with the dispersion $\delta\varepsilon_m = 0.3\omega_0$. The results of these calculations are illustrated by Fig. 7, which depicts 2D spectra for several population times T .

Let us first consider the left column of Fig. 7, which shows $S(\omega_\tau, T, \omega_t)$ calculated with the lineshape factors (30). At this level of description, the Markovian bath causes homogeneous broadening of spectral features, and disorder

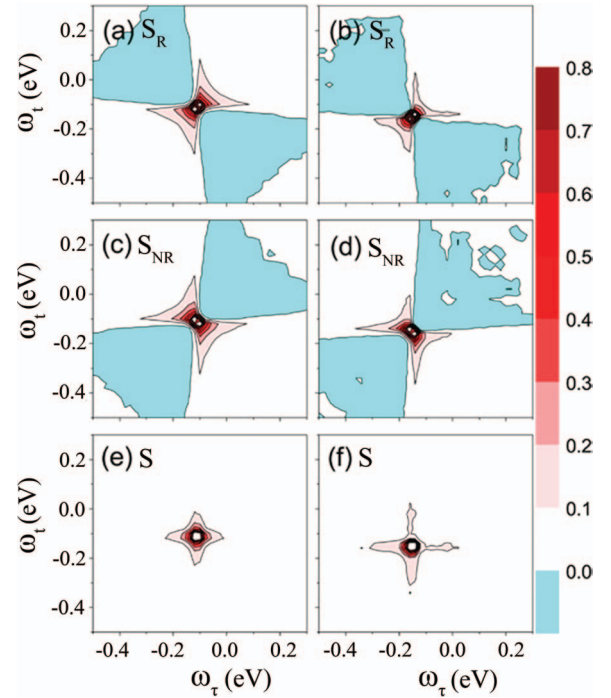


FIG. 6. 2D spectra at $T = 0$ calculated via D_1 Ansatz in the limit of Markovian bath-induced homogeneous broadening. The left column corresponds to the toy model ($S = 0.5$, $W = 0.8\hbar\omega_0$, $J = 0.3\hbar\omega_0$), while the right column is for the realistic model (see Sec. II D for details). The upper, middle, and lower panels correspond to the rephasing, non-rephasing, and total 2D spectra.

is the unique source of inhomogeneous broadening. The disorder-induced inhomogeneous broadening thus persists as the population time increases, as shown in Figs. 7(a), 7(c), and 7(e).

The right column of Fig. 7 depicts $S(\omega_\tau, T, \omega_t)$ computed with the Kubo lineshape function

$$g(t) = \frac{\chi}{\Gamma_K^2} [\exp(-\Gamma_K t) + \Gamma_K t - 1], \quad (31)$$

which is a classical (high-temperature) limit of the lineshape function (23) for the Drude spectral density (29). We assume “realistic” values of the parameters, $\Gamma_K = 0.25\omega_0$ and $\chi = 1.23\omega_0^2$, which yield strong bath-induced dephasing. It thus serves as the reason to why the peak shapes in the right column of Fig. 7 are much broader than those in the left column.

The Kubo lineshape function (31) corresponds to a non-Markovian bath. The ensuing lineshape factors (22) ensure inhomogeneously broadened peaks in 2D spectra at short population times ($T \ll 1/\Gamma_K$). At longer times ($T \gg 1/\Gamma_K$), the lineshape factors (22) recover their Markovian form (30), and the peaks become inhomogeneously broadened. Therefore, the bath-induced inhomogeneous broadening becomes less pronounced as T increases. On the other hand, the inhomogeneous broadening due to the static disorder is T -independent. We thus expect that the peaks become more homogeneously broadened as T increases. This is evident in Figs. 7(b), 7(d), and 7(f).

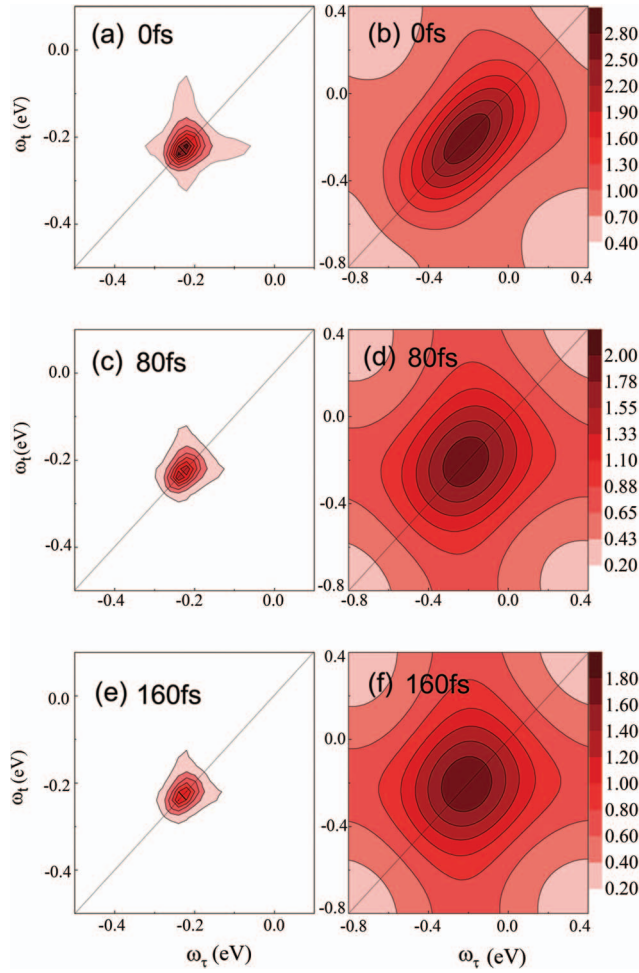


FIG. 7. Time evolution of 2D spectra for the realistic model of the molecular ring ($S = 0.5$, $W = 0.8\hbar\omega_0$) with Gaussian site-energy static disorder (the dispersion $\delta_m = 0.3\hbar\omega_0$). Left column corresponds to the Markovian lineshape factors (30), while the right column is for the Kubo lineshape model (31).

IV. CONCLUSION

We have developed a new approach to the computation of third-order spectroscopic signals of molecular rings, by incorporating the Davydov soliton theory into the nonlinear response function formalism. We have employed the Davydov D_1 and \tilde{D} *Ansätze* to treat the interaction between the excitons and the primary phonons. Our approach allows for strong exciton-phonon couplings and non-Markovian heat baths with arbitrary spectral densities. As an illustration, we have simulated a series of optical 2D spectra for two model molecular rings in the presence of intermediate and strong exciton-phonon coupling, exciton transfer integral, as well as bath-induced relaxation and dephasing. We hope that the developed approach may provide new insights into structural properties and relaxation dynamics of realistic excitonic systems.

ACKNOWLEDGMENTS

Support from the Singapore National Research Foundation through the Competitive Research Programme (CRP) un-

der Project No. NRF-CRP5-2009-04 is gratefully acknowledged. One of us (K.W.S.) also thanks NNSF of China (No. 11247238) for partial support.

APPENDIX: DETAILED DERIVATION OF EXCITON DYNAMICS IN ONE-RING SYSTEM

First, we take as an example the \tilde{D} *Ansatz* on a chromophore ring with only nearest-neighbor coupling to illustrate how the Dirac-Frenkel time-dependent variational procedure can be applied to reveal the polaron dynamics in a 1D system. For the \tilde{D} *Ansatz*, the dynamical behavior of the entire system can be determined if the time-dependent variation parameters $\alpha_m(t)$, $\beta_q(t)$, and $\lambda_q(t)$ are obtained. For this purpose, the Lagrangian is evaluated first, and the equations of motion for those variation parameters can be derived as

$$\frac{d}{dt} \left(\frac{\partial L}{\partial \dot{\alpha}_m^*} \right) - \frac{\partial L}{\partial \alpha_m^*} = 0, \quad (\text{A1})$$

$$\frac{d}{dt} \left(\frac{\partial L}{\partial \dot{\beta}_q^*} \right) - \frac{\partial L}{\partial \beta_q^*} = 0, \quad (\text{A2})$$

$$\frac{d}{dt} \left(\frac{\partial L}{\partial \dot{\lambda}_q^*} \right) - \frac{\partial L}{\partial \lambda_q^*} = 0, \quad (\text{A3})$$

where the Lagrangian L is formulated as follows:

$$\begin{aligned} L &= \langle \tilde{D}(t) | \frac{i\hbar}{2} \frac{\overleftrightarrow{\partial}}{\partial t} - \hat{H} | \tilde{D}(t) \rangle \\ &= \frac{i\hbar}{2} \left[\langle \tilde{D}(t) | \frac{\overrightarrow{\partial}}{\partial t} | \tilde{D}(t) \rangle - \langle \tilde{D}(t) | \frac{\overleftarrow{\partial}}{\partial t} | \tilde{D}(t) \rangle \right] \\ &\quad - \langle \tilde{D}(t) | \hat{H} | \tilde{D}(t) \rangle. \end{aligned} \quad (\text{A4})$$

Based on Eqs. (A1)–(A4), the time-dependent wave function $|\Psi_{\tilde{D}}(t)\rangle$ is determined. The equations of motion for the time-dependent variational parameters $\alpha_n(t)$, $\beta_q(t)$, and $\lambda_q(t)$ can be written as

$$\begin{aligned} -i\dot{\alpha}_n(t) &= \frac{i}{2} N^{-1} \alpha_n \sum_q \left[(\dot{\beta}_q e^{-iqn} - \dot{\lambda}_q) (\beta_q^* e^{iqn} - \lambda_q^*) \right. \\ &\quad \left. - (\beta_q^* e^{iqn} - \lambda_q^*) (\beta_q e^{-iqn} - \lambda_q) \right] \\ &\quad + J\alpha_{n+1} S_{n,n+1} + J\alpha_{n-1} S_{n,n-1} \\ &\quad - N^{-1} \alpha_n \sum_q \omega_q |\beta_q e^{-iqn} - \lambda_q|^2 \\ &\quad - N^{-1/2} \alpha_n \sum_q g_q \omega_q \\ &\quad \left[\beta_q^* - \lambda_q^* e^{iqn} + \beta_q - \lambda_q e^{iqn} \right], \end{aligned} \quad (\text{A5})$$

$$\begin{aligned}
-iN^{-1} \sum_n |\alpha_n|^2 \dot{\lambda}_q(t) &= -i \sum_n |\alpha_n|^2 \dot{\beta}_q e^{-iqn} N^{-1} \\
&+ \frac{1}{2} N^{-1} J \sum_n \alpha_n^* \alpha_{n+1} S_{n,n+1} \\
&\beta_q [e^{-iqn} - e^{-iq(n+1)}] \\
&+ \frac{1}{2} N^{-1} J \sum_n \alpha_n^* \alpha_{n-1} S_{n,n-1} \\
&\beta_q [e^{-iqn} - e^{-iq(n-1)}] \\
&+ N^{-1} \sum_n |\alpha_n|^2 \omega_q (\beta_q e^{-iqn} - \lambda_q) \\
&+ N^{-1/2} \sum_n |\alpha_n|^2 g_q \omega_q e^{-iqn}, \quad (\text{A6})
\end{aligned}$$

$$\begin{aligned}
-iN^{-1} \sum_n |\alpha_n|^2 \dot{\beta}_q &= -iN^{-1} \sum_n |\alpha_n|^2 \dot{\lambda}_q e^{iqn} \\
&+ JN^{-1} \sum_n \alpha_n^* \alpha_{n+1} S_{n,n+1} \\
&\left[\beta_q (e^{-iq} - 1) + \frac{1}{2} \lambda_q e^{iqn} (e^{iq} - 1) \right] \\
&+ JN^{-1} \sum_n \alpha_n^* \alpha_{n-1} S_{n,n-1} \\
&\left[\beta_q (e^{iq} - 1) + \frac{1}{2} \lambda_q e^{iqn} (e^{-iq} - 1) \right] \\
&- N^{-1} \sum_n |\alpha_n|^2 \omega_q (\beta_q - \lambda_q e^{iqn}) \\
&- N^{-1/2} \sum_n |\alpha_n|^2 g_q \omega_q, \quad (\text{A7})
\end{aligned}$$

with

$$\begin{aligned}
S_{n,m} &= \exp \left[-\frac{1}{2} N^{-1} \sum_q |\beta_q e^{-iqn} - \lambda_q|^2 \right] \\
&\exp \left[-1/2 N^{-1} \sum_q |\beta_q e^{-iqm} - \lambda_q|^2 \right] \\
&\exp \left[N^{-1} \sum_q (\beta_q^* e^{iqn} - \lambda_q^*) \right. \\
&\left. (\beta_q e^{-iqm} - \lambda_q) \right]. \quad (\text{A8})
\end{aligned}$$

Next, we move on to the more sophisticated D_1 Ansatz and derive the equation of motions of the variational parameters for polaronic dynamics in a chromophore ring with long-range interactions J_{mn} . A similar procedure will be followed once the Lagrangian is evaluated for the D_1 Ansatz. The equations of motions for the time-dependent variational parameters $\alpha_n(t)$ and $\lambda_{nq}(t)$ can be obtained as

$$\dot{\alpha}_n(t) = i[T_n(t) + \alpha_n(t)R_n(t)], \quad (\text{A9})$$

and

$$\dot{\lambda}_{nq}(t) = i \left[\frac{\Omega_{nq}(t)}{\alpha_n(t)} + \frac{g_q}{\sqrt{N}} \omega_q e^{-iqn} - \omega_q \lambda_{nq}(t) \right]. \quad (\text{A10})$$

Auxiliary functions introduced term in Eqs. (A9) and (A10) are given as

$$\varpi_{nq}(t) = i \dot{\lambda}_{nq}(t) + \frac{g_q}{\sqrt{N}} \omega_q e^{-iqn} - \omega_q \lambda_{nq}(t), \quad (\text{A11})$$

$$R_n(t) = \text{Re} \sum_q \left[\varpi_{nq}(t) + \frac{g_q}{\sqrt{N}} \omega_q e^{-iqn} \right] \lambda_{nq}^*(t), \quad (\text{A12})$$

$$T_n(t) = \sum_m J_{nm} \alpha_m(t) S_{nm}(t), \quad (\text{A13})$$

$$\Omega_{nq}(t) = \sum_m J_{nm} \alpha_m(t) S_{nm}(t) [\lambda_{mq}(t) - \lambda_{nq}(t)], \quad (\text{A14})$$

with the Debye-Waller factor $S_{nm}(t)$ given by

$$\begin{aligned}
S_{nm}(t) &= \exp \left\{ \sum_q \left[\lambda_{nq}^*(t) \lambda_{mq}(t) \right. \right. \\
&\left. \left. - \frac{1}{2} |\lambda_{nq}(t)|^2 - \frac{1}{2} |\lambda_{mq}(t)|^2 \right] \right\}. \quad (\text{A15})
\end{aligned}$$

¹G. D. Scholes, G. R. Fleming, A. Olaya-Castro, and R. van Grondelle, *Nat. Chem.* **3**, 763–774 (2011).

²Y. C. Cheng and G. R. Fleming, *Annu. Rev. Phys. Chem.* **60**, 241–262 (2009).

³A. Camara-Artigas, R. E. Blankenship, and J. P. Allen, *Photosynth. Res.* **75**, 49–55 (2003).

⁴Y. Zhao, M. F. Ng, and G. H. Chen, *Phys. Rev. E* **69**, 032902 (2004); M. F. Ng, Y. Zhao, and G. H. Chen, *J. Phys. Chem. B* **107**, 9589 (2003).

⁵Y. Zhao, T. Meier, W. M. Zhang, V. Chernyak, and S. Mukamel, *J. Phys. Chem. B* **103**, 3954 (1999); T. Meier, Y. Zhao, V. Chernyak, and S. Mukamel, *J. Chem. Phys.* **107**, 3876 (1997).

⁶S. Mukamel, *Principles of Nonlinear Optical Spectroscopy* (Oxford University Press, New York, 1995).

⁷H. van Amerongen, L. Valkunas, and R. van Grondelle, *Photosynthetic Excitations* (World Scientific, Singapore, 2000).

⁸T. Renger, V. May, and O. Kühn, *Phys. Rep.* **343**, 137 (2001).

⁹D. Abramavicius, B. Palmieri, D. V. Voronine, F. Šanda, and S. Mukamel, *Chem. Rev.* **109**, 2350 (2009).

¹⁰K. Hyeon-Deuk and Y. Tanimura, *J. Chem. Phys.* **127**, 075101 (2007).

¹¹V. Butkus, A. Gelzinis, and L. Valkunas, *J. Phys. Chem. A* **115**, 3876 (2011).

¹²A. Gelzinis, D. Abramavicius, and L. Valkunas, *Phys. Rev. B* **84**, 245430 (2011).

¹³M. Khalil, N. Demirdöven, and A. Tokmakoff, *J. Phys. Chem. A* **107**, 5258 (2003).

¹⁴A. G. Dijkstra, T. la C. Jansen, and J. Knoester, *J. Chem. Phys.* **128**, 164511 (2008).

¹⁵I. Stiopkin, T. Brixner, M. Yang, and G. R. Fleming, *J. Phys. Chem. B* **110**, 20032 (2006).

¹⁶G. S. Engel, T. R. Calhoun, E. L. Read, T. K. Ahn, T. Mančal, Y. C. Cheng, R. E. Blankenship, and G. R. Fleming, *Nature (London)* **446**, 782 (2007).

¹⁷M. Cho, H. M. Vaswani, T. Brixner, J. Stenger, and G. R. Fleming, *J. Phys. Chem. B* **109**, 10542 (2005).

¹⁸P. Kjellberg, B. Brügemann, and T. Pullerits, *Phys. Rev. B* **74**, 024303 (2006).

¹⁹F. Milota, J. Sperling, A. Nemeth, D. Abramavicius, S. Mukamel, and H. F. Kauffmann, *J. Chem. Phys.* **131**, 054510 (2009).

²⁰J. M. Womick, S. A. Miller, and A. M. Moran, *J. Phys. Chem. A* **113**, 6587 (2009).

- ²¹J. M. Womick, S. A. Miller, and A. M. Moran, *J. Phys. Chem. B* **113**, 6630 (2009).
- ²²N. S. Ginsberg, Y. C. Cheng, and G. R. Fleming, *Acc. Chem. Res.* **42**, 1352 (2009).
- ²³D. Egorova, M. F. Gelin, and W. Domcke, *J. Chem. Phys.* **126**, 074314 (2007).
- ²⁴H. S. Tan, *J. Chem. Phys.* **129**, 124501 (2008).
- ²⁵T.-S. Ahn, A. M. Müller, R. O. Al-Kaysi, F. C. Spano, J. E. Norton, D. Beljonne, J.-L. Brédas, and C. J. Bardeen, *J. Chem. Phys.* **128**, 054505 (2008).
- ²⁶K. Hyeon-Deuk, Y. Tanimura, and M. Cho, *J. Chem. Phys.* **128**, 135102 (2008).
- ²⁷J. R. Durrant, J. Knoester, and D. A. Wiersma, *Chem. Phys. Lett.* **222**, 450 (1994).
- ²⁸D.-J. Heijs, A. G. Dijkstra, and J. Knoester, *Chem. Phys.* **341**, 230–239 (2007).
- ²⁹L. D. Bakalis and J. Knoester, *J. Phys. Chem. B* **103**, 6620 (1999).
- ³⁰H. Fidder, J. Knoester, and D. A. Wiersma, *Chem. Phys. Lett.* **171**, 529 (1990).
- ³¹S. de Boer, K. J. Vink, and D. A. Wiersma, *Chem. Phys. Lett.* **137**, 99 (1987).
- ³²S. de Boer and D. A. Wiersma, *Chem. Phys. Lett.* **165**, 45 (1990).
- ³³K. A. Merchant, D. E. Thompson, and M. D. Fayer, *Phys. Rev. Lett.* **86**, 3899 (2001).
- ³⁴D. E. Thompson, K. A. Merchant, and M. D. Fayer, *J. Chem. Phys.* **115**, 317 (2001).
- ³⁵P. Hamm, M. Lim, W. F. DeGrado, and R. Hochstrasser, *J. Phys. Chem. A* **103**, 10049 (1999).
- ³⁶S. Mukamel and D. Abramavicius, *Chem. Rev.* **104**, 2073 (2004).
- ³⁷M. Cho, *Two-Dimensional Optical Spectroscopy* (CRC Press, New York, 2009).
- ³⁸C. Liand and T. L. C. Jansen, *J. Chem. Theory Comput.* **8**, 1706 (2012).
- ³⁹W. Domcke and G. Stock, *Adv. Chem. Phys.* **100**, 1 (1997).
- ⁴⁰M. F. Gelin, D. Egorova, and W. Domcke, *Acc. Chem. Res.* **42**, 1290 (2009).
- ⁴¹H. D. Meyer, *Comput. Mol. Sci.* **2**, 351 (2012).
- ⁴²Q. Y. Meng and H.-D. Meyer, *J. Chem. Phys.* **138**, 014313 (2013).
- ⁴³H. Wang and M. Thoss, *Chem. Phys.* **347**, 139 (2008).
- ⁴⁴B. Brüggemann, P. Petersson, H.-D. Meyer, and V. May, *Chem. Phys.* **347**, 152 (2008).
- ⁴⁵H.-P. Breuer and F. Petruccione, *The Theory of Open Quantum Systems* (Oxford University Press, New York, 2002).
- ⁴⁶V. May and O. Kühn, *Charge and Energy Transfer Dynamics in Molecular Systems* (Wiley-VCH, Berlin, 2004).
- ⁴⁷A. Ishizaki and Y. Tanimura, *Chem. Phys.* **347**, 185 (2008).
- ⁴⁸R. X. Xu, B. L. Tian, J. Xu, Q. Shi, and Y. J. Yan, *J. Chem. Phys.* **131**, 214111 (2009).
- ⁴⁹Y. Tanimura, *J. Phys. Soc. Jpn.* **75**, 082001 (2006).
- ⁵⁰B. Hein, C. Kreisbeck, T. Kramer, and M. Rodriguez, *New J. Phys.* **14**, 023018 (2012).
- ⁵¹Y.-C. Cheng and R. J. Silbey, *J. Chem. Phys.* **128**, 114713 (2008).
- ⁵²S. Jang, Y.-C. Cheng, D. R. Reichman, and J. D. Eaves, *J. Chem. Phys.* **129**, 101104 (2008).
- ⁵³Spectroscopic signatures of small polarons have recently been measured by nonlinear vibrational spectroscopy.^{54,55}
- ⁵⁴J. Edler, R. Pfister, V. Pouthier, C. Falvo, and P. Hamm, *Phys. Rev. Lett.* **93**, 106405 (2004).
- ⁵⁵P. Bodis, E. Schwartz, M. Koepf, J. J. L. M. Cornelissen, A. E. Rowan, R. J. M. Nolte, and S. Woutersen, *J. Chem. Phys.* **131**, 124503 (2009).
- ⁵⁶S.-H. Yeh, J. Zhu, and S. Kais, *J. Chem. Phys.* **137**, 084110 (2012).
- ⁵⁷A. S. Davydov and N. I. Kislukha, *Phys. Status Solidi B* **59**, 465 (1973).
- ⁵⁸A. S. Davydov, *Solitons in Molecular Systems* (Reidel, Dordrecht, 1985).
- ⁵⁹M. J. Šrinjar, D. V. Kapor and S. D. Stojanović, *Phys. Rev. A* **38**, 6402 (1988).
- ⁶⁰L. Cruzeiro-Hansson, *Phys. Rev. Lett.* **73**, 2927 (1994).
- ⁶¹J. Sun, B. Luo, and Y. Zhao, *Phys. Rev. B* **82**, 014305 (2010).
- ⁶²B. Luo, J. Ye, C. B. Guan, and Y. Zhao, *Phys. Chem. Chem. Phys.* **12**, 15073 (2010); Y. Yao, L. W. Duan, Z. G. Lu, C. Q. Wu, and Y. Zhao, *Phys. Rev. E* **88**, 023303 (2013); Y. Yao and Y. Zhao, *J. Chem. Phys.* **139**, 014102 (2013).
- ⁶³G. C. Yang, N. Wu, T. Chen, K. W. Sun, and Y. Zhao, *J. Phys. Chem. C* **116**, 3747 (2012).
- ⁶⁴J. Ye, K. W. Sun, Y. Zhao, Y. J. Yu, C. K. Lee, and J. S. Cao, *J. Chem. Phys.* **136**, 245104 (2012).
- ⁶⁵B. Luo, J. Ye, and Y. Zhao, *Phys. Status Solidi C* **8**, 70 (2011).
- ⁶⁶A. Damjanović, I. Kosztin, U. Kleinekathöfer, and K. Schulten, *Phys. Rev. E* **65**, 031919 (2002).
- ⁶⁷V. Chernyak and S. Mukamel, *J. Chem. Phys.* **105**, 4565 (1996).
- ⁶⁸M. Thoss, H. Wang, and W. H. Miller, *J. Chem. Phys.* **115**, 2991 (2001).
- ⁶⁹K. H. Hughes, C. D. Christ, and I. Burghardt, *J. Chem. Phys.* **131**, 024109 (2009).
- ⁷⁰K. H. Hughes, C. D. Christ, and I. Burghardt, *J. Chem. Phys.* **131**, 124108 (2009).
- ⁷¹M. F. Gelin, D. Egorova, and W. Domcke, *J. Chem. Phys.* **136**, 034507 (2012).
- ⁷²G. D. Mahan, *Many Particle Physics*, 3rd ed. (Springer, Dordrecht, 2000).
- ⁷³P. A. M. Dirac, *Proc. Cambridge Philos. Soc.* **26**, 376 (1930); J. Frenkel, *Wave Mechanics* (Oxford University Press, New York, 1934).
- ⁷⁴R. Doll, D. Zueco, M. Wubs, S. Kohler, and P. Hänggi, *Chem. Phys.* **347**, 243 (2008).
- ⁷⁵M. F. Gelin, D. Egorova, and W. Domcke, *Phys. Rev. E* **84**, 041139 (2011).
- ⁷⁶R. M. Hochstrasser, *Chem. Phys.* **266**, 273 (2001).
- ⁷⁷A. Tokmakoff, *J. Chem. Phys.* **105**, 1 (1996).
- ⁷⁸D. Abramavicius, B. Palmieri, and S. Mukamel, *Chem. Phys.* **357**, 79 (2009).
- ⁷⁹C. Olbrich, T. L. C. Jansen, J. Liebers, M. Aghtar, J. Strümfel, K. Schulten, J. Knoester, and U. Kleinekathöfer, *J. Phys. Chem. B* **115**, 8609 (2011).
- ⁸⁰P. Xiao-Feng, *Phys. Rev. E* **62**, 6989 (2000).
- ⁸¹L. Cruzeiro-Hansson, *Phys. Rev. E* **66**, 023901 (2002).
- ⁸²D. Kapor, M. Skrinjar, Z. Ivic, and Z. Przulj, *Phys. Rev. E* **73**, 013901 (2006).
- ⁸³N. Christensson, F. Milota, J. Hauer, J. Sperling, O. Bixner, A. Nemeth, and H. F. Kauffmann, *J. Phys. Chem. B* **115**, 5383 (2011).
- ⁸⁴D. B. Turner, K. E. Wilk, P. M. G. Curmi, and G. D. Scholes, *J. Phys. Chem. Lett.* **2**, 1904 (2011).
- ⁸⁵K. A. Fransted and G. S. Engel, *Chem. Phys.* **403**, 59 (2012).
- ⁸⁶J. Yuen-Zhou, J. J. Krich, and A. Aspuru-Guzik, *J. Chem. Phys.* **136**, 234501 (2012).
- ⁸⁷T. Mančal, N. Christensson, V. Lukeš, F. Milota, O. Bixner, H. F. Kauffmann, and J. Hauer, *J. Phys. Chem. Lett.* **3**, 1497 (2012).
- ⁸⁸N. Christensson, H. F. Kauffmann, T. Pullerits, and T. Mančal, *J. Phys. Chem. B* **116**, 7449 (2012).
- ⁸⁹T. Pullerits, D. Zigmantas, and V. Sundström, *Proc. Natl. Acad. Sci. U.S.A.* **110**, 1148 (2013).
- ⁹⁰V. Tiwari, W. K. Petdr, and D. M. Jonas, *Proc. Natl. Acad. Sci. U.S.A.* **110**, 1203 (2013).
- ⁹¹V. Butkus, D. Zigmantas, L. Valkunas, and D. Abramavicius, *Chem. Phys. Lett.* **545**, 40 (2012).
- ⁹²W. S. Struve, *Biophys. J.* **69**, 2739 (1995).
- ⁹³M. Rätser, Z.-L. Cai, J. R. Reimers, and A. Freiberg, *J. Chem. Phys.* **134**, 024506 (2011).
- ⁹⁴Y. Jing, R. Zheng, H.-X. Li, and Q. Shi, *J. Phys. Chem. B* **116**, 1164 (2012).
- ⁹⁵T. Renger and R. A. Marcus, *J. Chem. Phys.* **116**, 9997 (2002).
- ⁹⁶S. Jang and R. J. Silbey, *J. Chem. Phys.* **118**, 9324 (2003).
- ⁹⁷L. Janosi, I. Kosztin, and A. Damjanović, *J. Chem. Phys.* **125**, 014903 (2006).
- ⁹⁸D. Egorova, M. F. Gelin, and W. Domcke, *Chem. Phys.* **341**, 113 (2007).
- ⁹⁹S. M. G. Faeder and D. M. Jonas, *J. Phys. Chem. A* **103**, 10489 (1999).
- ¹⁰⁰T. Mančal, A. Nemeth, F. Milota, V. Lukeš, H. F. Kauffmann, and J. Sperling, *J. Chem. Phys.* **132**, 184515 (2010).
- ¹⁰¹V. Butkus, L. Valkunas, and D. Abramavicius, *J. Chem. Phys.* **137**, 044513 (2012).
- ¹⁰²A. Schubert and V. Engel, *J. Chem. Phys.* **134**, 104304 (2011).
- ¹⁰³D. Egorova, *Chem. Phys.* **347**, 166 (2008).
- ¹⁰⁴Y. Tanimura, *J. Chem. Phys.* **137**, 22A550 (2012).
- ¹⁰⁵J. Krčmář, M. F. Gelin, and W. Domcke, *Chem. Phys.* **422**, 53 (2013).
- ¹⁰⁶J. Seibt, K. Renziehausen, D. V. Voronine, and V. Engel, *J. Chem. Phys.* **130**, 134318 (2009).
- ¹⁰⁷J. Seibt and A. Eisfeld, *J. Chem. Phys.* **136**, 024109 (2012).